water

MDPI

Article

Characteristics of Evapotranspiration and Water Consumption of Different Underlying Surfaces in Qaidam Basin

Yuanzheng Wang [1], Caizhi Hu [1], Xiaopeng Jia [1,*] and Qimin Ma [2]

[1] Key Laboratory of Desert and Desertification, Northwest Institute of Eco-Environment and Resources, Chinese Academy of Sciences, Lanzhou 730000, China
[2] College of Resources and Environment, Chengdu University of Information Technology, Chengdu 610225, China
* Correspondence: jiaxp@lzb.ac.cn

Abstract: The Qaidam Basin is an alpine arid inland basin characterized by water resource shortages and fragile ecological environments. Studying the evapotranspiration and water consumption characteristics of the Qaidam Basin is important for regional water-resource management and environmental protection. Based on eddy covariance flux data for four underlying surfaces (Golmud cropland, shrubland, Nomuhong cropland, and alpine meadow) in the Qaidam Basin in 2020, the evapotranspiration variation characteristics for different underlying surfaces at different time scales were analyzed, the influence of different typical meteorological factors on actual evapotranspiration was explored, and water consumption characteristics of the different underlying surfaces were analyzed. The results showed that the evapotranspiration of each underlying surface was mainly concentrated in the growing season. The Golmud cropland and alpine meadow had the highest evapotranspiration in July, at 62.50 mm and 88.92 mm, respectively, while the shrubland and Nomuhong cropland had the highest evapotranspiration in August, at 40.47 mm and 100.02 mm, respectively. The average daily evapotranspiration of Golmud cropland, shrubland, Nomuhong cropland, and alpine meadow was 1.12 mm, 0.78 mm, 1.98 mm, and 1.79 mm, respectively. The half-hour evapotranspiration reached a maximum value from 14:00–15:00. The evapotranspiration of different underlying surfaces was strongly correlated with air temperature, followed by relative humidity, and weakly correlated with wind speed. Daily evapotranspiration was strongly correlated with the soil temperature of Golmud cropland, shrubland, and alpine meadow, and the soil volume water content of shrubland and alpine meadows. The water consumption variation characteristics indicated that each underlying surface was dominated by water consumption, accounting for 96.73%, 96.26%, 96.26%, 74.30% in Golmud cropland, shrubland, Nomuhong cropland, and alpine meadow, respectively. Among them, precipitation was the main factor affecting the water consumption of the different underlying surfaces. The purpose of this study was to explore the actual evapotranspiration characteristics of different underlying surfaces, the results of which can be used as a reference for studies of the water cycle in Qaidam Basin.

Keywords: actual evapotranspiration; Qaidam Basin; eddy covariance; meteorological factors; water consumption

check for updates

Citation: Wang, Y.; Hu, C.; Jia, X.; Ma, Q. Characteristics of Evapotranspiration and Water Consumption of Different Underlying Surfaces in Qaidam Basin. *Water* **2022**, *14*, 3469. https://doi.org/10.3390/w14213469

Academic Editor: Achim A. Beylich

Received: 28 September 2022
Accepted: 27 October 2022
Published: 30 October 2022

Publisher's Note: MDPI stays neutral with regard to jurisdictional claims in published maps and institutional affiliations.

Copyright: © 2022 by the authors. Licensee MDPI, Basel, Switzerland. This article is an open access article distributed under the terms and conditions of the Creative Commons Attribution (CC BY) license (https://creativecommons.org/licenses/by/4.0/).

1. Introduction

Evapotranspiration (ET), which includes water evaporation at the soil and vegetation surface and transpiration of vegetation [1], is involved in the conversion of water in a soil-vegetation-atmosphere continuum (SPAC) and represents an important key component of the balance between water and energy [2,3]. Moreover, ET is a significant factor that affects micro-meteorological conditions at a small scale and climate change at a large scale, and it is influenced by multiple aspects of the environment and biological systems [4]. Semi-arid and arid regions cover at least one-third of the global land surface and constitute an important

part of the global ecosystem [5]. Approximately 60% of global precipitation returns to the atmosphere through ET [6,7], and this value is more than 90% in arid and semi-arid regions [8]. In recent decades, an increasing number of studies have been conducted on ET in arid areas [9–11]. Previous studies have shown that ET is very sensitive to temperature, relative humidity, and other environmental factors [12,13] and it differs based on different underlying surfaces [14]. With the influence of climate change and human activities, changes in soil type, water conditions, land use, and vegetation will affect the change in ET, especially meteorological factors that directly control the ET rate [15]. Therefore, changes in ET in arid areas should be studied to improve water resource management and monitor climate change [16,17].

ET acquisition methods mainly include ground-based observation and model estimation. The ET estimation models available in the literature may be classified as (1) fully physically based combination models that account for mass and energy conservation principles; (2) semi-physically based models that deal with either mass or energy conservation; and (3) black-box models based on artificial neural networks, empirical relationships, and fuzzy and genetic algorithms [18,19]. In terms of model estimations, remote sensing technology has many advantages, being rapid, convenient, and macroscopic, and has incomparable advantages in obtaining regional surface characteristic parameters, and so has become the mainstream method for large-scale land ET estimation [20,21]. However, because of the complexity of surface processes, remote sensing technology has certain limiting factors, such as the model mechanism, model inputs, parameterization schemes, and scaling issues [22–24]. Therefore, the accuracy of remote sensing ET model simulation results must be evaluated based on ground observation data to improve the model.

In recent decades, the methods commonly used to measure ET include the weighing lysimeter method [25], the Bovenby-energy balance method [26], and the eddy covariance method (EC) [27]. Compared with other methods, the EC method has a complete physical basis and fewer theoretical assumptions and thus provides a direct measurement of water vapor exchange between terrestrial ecosystems and the atmosphere [28,29]. Based on the popularity of the EC method worldwide, a global-scale network of flux measurements, FLUXNET, was established in 1998, and it covers a variety of terrestrial ecosystems, including forests, grasslands, agricultural ecosystems, wetlands, and deserts, and provides a large amount of data for the global water cycle [30–32]. The EC flux data of different land cover types can effectively improve model algorithms and verify products derived from remote sensing ET models [33,34]. However, because of the wide variety of underlying surface types, the FLUXNET observation sites are unevenly distributed in terms of space and vegetation types. Thus, new observation stations need to be built to increase the representativeness of the data.

The Qaidam Basin is a typical alpine and arid inland basin characterized by cold temperatures, an arid and windy climate, sandy substrates, high salinity, water shortages, spatiotemporally uneven water distributions, concentrated resource development, serious desertification, and a fragile ecological environment. Because of the harsh natural conditions of the Qaidam Basin, actual observational data are limited; therefore, few studies have focused on the ET in the area. Remote sensing technology is primarily used to obtain ET data. For example, Jin et al. estimated the ET of the Qaidam Basin, and eight tertiary water resource regions based on remote sensing data and analyzed the influencing factors [9], while Guo et al. used medium-resolution remote sensing data to estimate the actual ET of the Qaidam Basin and performed a comparative analysis of the ET of different land-use types [35]. Although the above research analyzed the large-scale spatial distribution characteristics of ET in the Qaidam Basin through remote sensing ET models, pan evaporation and evaporation coefficients were used to verify the simulation results, while the evaporation measured by the evaporation pan was used to verify the water surface evaporation. Therefore, long-term ground-based observation on actual ET of various land covers are needed to evaluate and improve the reliability of the model. These studies will fill the gap in the actual ET of different underlying surfaces in this region.

Previous studies on ET in the Qaidam Basin mainly relied on model simulations, and direct calculations of the actual ET on different underlying surfaces are lacking. Therefore, the actual ET of four observation stations in the Qaidam Basin was calculated using the latent heat data observed by EC, and the actual ET variation characteristics of different underlying surfaces, including *Lycium barbarum* in sandy land, shrubland, and *Lycium barbarum* in large cropland areas, and alpine meadows, were analyzed at different time scales. The influence of meteorological factors, such as temperature, relative humidity, and wind speed on the actual ET was discussed, and the water consumption characteristics of different underlying surfaces were compared through the relationship between ET and precipitation, which provided a reference and data support for studies on the water cycle in the Qaidam Basin.

2. Materials and Methods

2.1. Study Area and Site Description

The Qaidam Basin is located in the northwest of Qinghai Province from 90°16′–99°16′ E, 35°00′–39°20′ N (Figure 1), and it is surrounded by the Altun Mountains in the northwest, Qilian Mountains in the northeast, and Kunlun Mountains in the south.

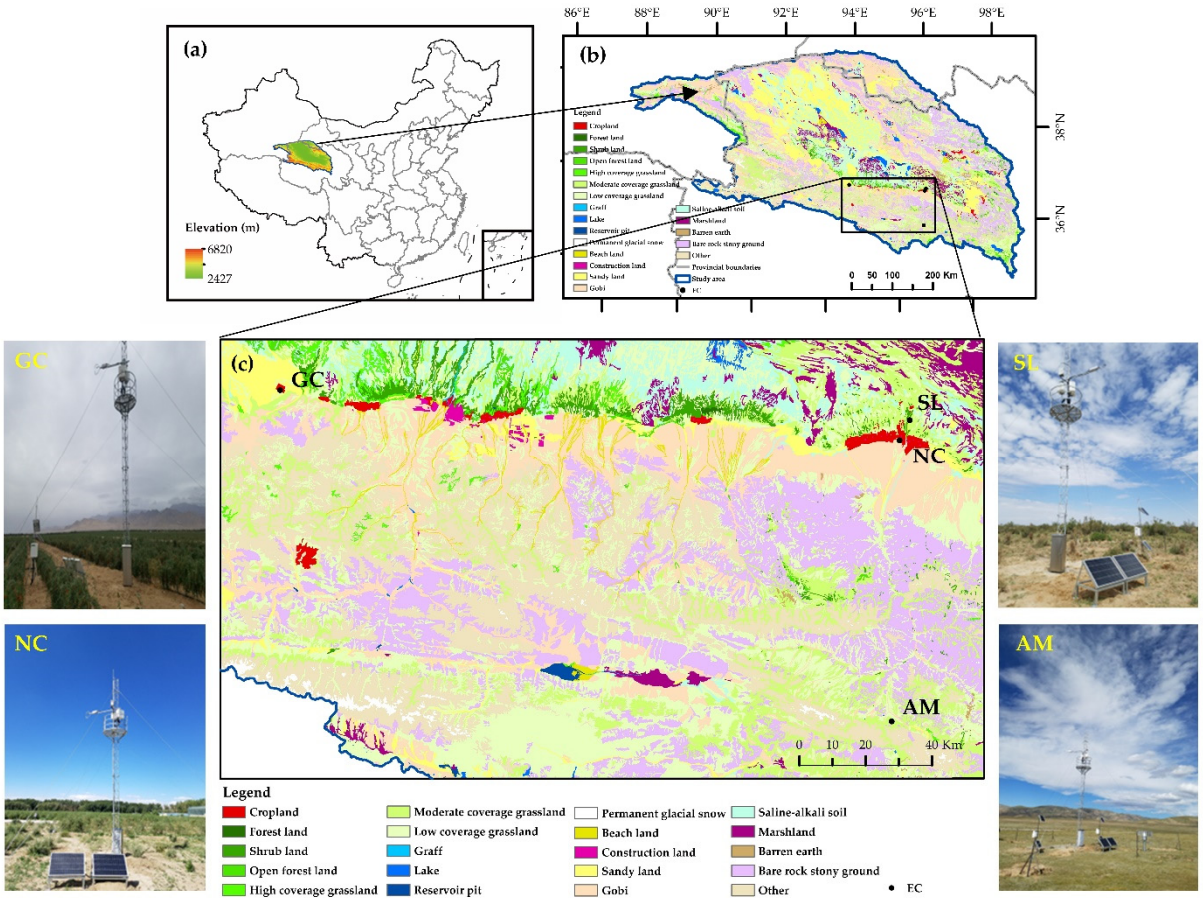

Figure 1. (**a**) The location and elevation of the study area and (**b**,**c**) spatial distribution of 4 observation sites in Qaidam Basin in 2020.

The Qaidam Basin is the largest inland basin in China. The basin covers an area of 275,000 km^2 with an average elevation of above 3000 m. The basin is located at the junction of the mid-latitude westerly belt and the East Asian monsoon system, which is an arid area in Northwest China. The climate is a typical plateau continental climate that presents cold, dry, and windy conditions and strong solar radiation. The precipitation is less than 200 mm overall and less than 25 mm at the center of the basin, and the precipitation decreases

from the mountain area to the interior of the basin [36]. The main vegetation types in the Qaidam Basin are grasslands, shrubs, and deserts [37]. The vegetation growing season is from May to September, during which the monthly average temperature is above 0 °C, and the precipitation in this period accounts for more than 90% of the annual total.

In this study, one station was set up in the mountainous area of the Qaidam Basin and three stations were set up in the plain area of the basin. The spatial distribution is shown in Figure 1. The Golmud cropland station (GC) is located in Golmud City and covers an area of 500 ha of cultivated *Lycium barbarum* in a sandy land area; the shrubland station (SL) is covered by Tamarix ramosissima and wild *Lycium barbarum*; the Nuomuhong cropland station (NC) is located in Dulan County, Nuomuhong township, and covers an area of 5000 ha of cultivated *Lycium barbarum*; and the alpine meadow station (AM) is covered by alpine meadow. Details of the EC system equipment at the four observation stations are listed in Table 1.

A T200B weighting rain and snow measurement system was used to measure the long-term precipitation on the underlying surface. The soil temperature, volume water content, and salinity sensor (CS655) probe were installed at 10 soil depths and spaced 10 cm to 100 cm apart, and data were automatically recorded every 10 min.

Table 1. Information of 4 observation stations and instruments in Qaidam Basin in 2020.

Site Name (Abbreviations)	Longitude, Latitude	Altitude (m)	Turbulence Sensors, Manufacturers	Sensor Hight (m)	Surface Type	Duration
Golmud cropland station (GC)	94°17′54.30″ E 36°24′45.87″ N	2790	CAT3A&EC155, Campbell, Logan, UT, USA	8	*Lyceum barbarum*	January–December 2020
Shrubland station (SL)	96°27′18.42″ E 36°29′44.07″ N	2732	CAT3A&EC155, Campbell, Logan, UT, USA	8	*Tamarix chinensis* and wild *Lycium barbarum*	January–December 2020
Nuomuhong cropland station (NC)	96°25′35.42″ E 36°26′23.36″ N	2775	CAT3A&EC155, Campbell, Logan, UT, USA	8	*Lycium barbarum*	January–December 2020
Alpine meadow station (AM)	96°28′56.00″ E 35°41′20.85″ N	4186	CAT3A&EC155, Campbell, Logan, UT, USA	8	*Alpine meadow*	January–November 2020

2.2. Flux Data Processing and Missing Data Interpolation

The basic process of processing raw 10 Hz EC data includes four steps: (1) Loggernet software was used for format conversion and data segmentation of the original 10 Hz data to obtain flux data every 30 min; (2) EddyPro software (Version 7.0, LiCOR Biosciences, Lincoln, NE, USA) was used for correction processing and quality control of the converted data [38], including outlier elimination, delay time correction, tilt correction (quadratic coordinate rotation), frequency response correction, ultrasonic virtual temperature correction, and density correction (WPL) correction. Quality control was divided into three grades (0, 1, and 2) by evaluating the flux value using two standards: a turbulence stability test and a turbulence development test; (3) Data were further screened according to the quality labeling and observation data, and flux data in the precipitation period were excluded, including poor quality data (labeled as 2) and insufficient turbulence development at night (friction wind speed less than 0.1 m/s) [39]; and (4) Missing data were interpolated using a linear interpolation method if the missing data occurred over less than 2 h and the mean diurnal variation (MDV) method if the missing data occurred over more than 2 h [40]. Thus, the average observation values in the same period of 7 to 10 days were used for interpolation. Finally, complete time-series flux data were obtained.

2.3. Calculation of Evapotranspiration

EC technology can directly measure the latent heat flux at different underlying surfaces. To obtain the half-hour ET (ET, mm/30 min) data of the ecosystem, after processing the raw data, the following formula should be used for calculation:

$$ET = \frac{1800LE}{\lambda}, \quad (1)$$

where LE is the latent heat flux (W/m^2) and λ is the latent heat of vaporization of water (J/kg).

2.4. Analysis of Correlation

In this study, IMB SPSS Statistics software (version 20.0, IBM Corp., Armonk, NY, USA) was used to perform Pearson correlation analyses between ET and air temperature, relative humidity, wind speed, soil temperature, and soil volume water content.

2.5. Water Consumption of Underlying Surface

Underlying surface water consumption (IETP) refers to the difference between ET and precipitation (Pr) over the underlying surface, which reflects the characteristics of water vapor exchange between the underlying surface and the atmosphere. The formula used is as follows:

$$IETP = ET - Pr, \quad (2)$$

when $IETP \geq 0$, the water vapor exchange characteristics of the underlying surface are mainly water consumption; and when $IETP < 0$, the water vapor exchange characteristics of the underlying surface are mainly water absorption [41].

3. Results and Discussion

3.1. Meteorological Conditions

Figure 2 shows the monthly changes in the environmental factors at the four observation stations in the Qaidam Basin (some stations have missing data). Overall, the meteorological factors of AM located in the mountainous area were very different from those of the three stations located in the basin plain area. The temperature of different underlying surfaces over one to seven months slowly rose, reached a maximum value in July, and then began to decline. The temperatures of the three observation stations located in the basin plain area of GC, SL, and NC were not very different, and the change range was between −10 and 20 °C; however, the temperature of the AM in the mountainous area was approximately 5 to 10 °C lower than that of the other three stations, and the change range was between −15 and 10 °C. The relative humidity of GC, SL, and NC throughout the year was almost less than 40%, while that of AM was more than 40%. There were certain differences in the wind speed changes of the four observation stations, among which the fluctuation range of the SL was large. The precipitation in GC, SL, and NC was generally less than 10 cm and scarce, while the maximum precipitation in AM reached 116 mm in June. The variation trends in soil temperature and air temperature at different stations were roughly the same. The variation range of soil temperature at GC and SL was −5 to 20 °C, and that at AM was −15 to 10 °C. The soil volume water content (VWC) of GC was below 0.1, whereas that of AM was between 0 and 0.3, thus showing a trend of increasing first and then decreasing.

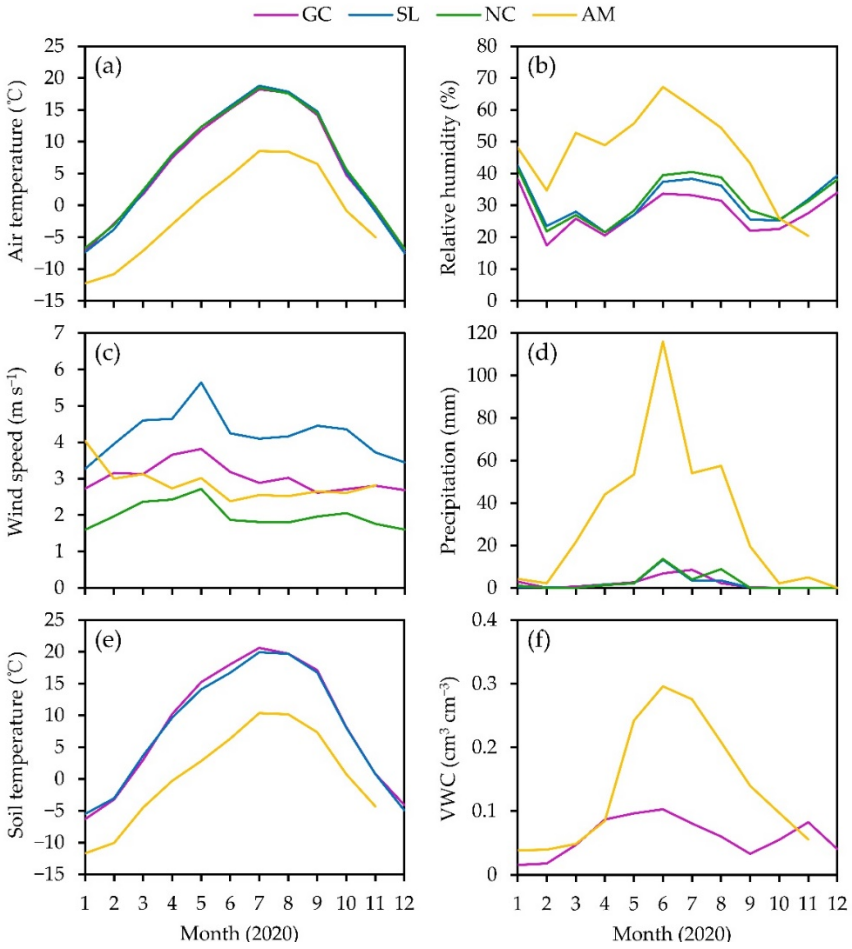

Figure 2. Monthly variation of different environmental factors at four observation stations in the Qaidam Basin in 2020. Monthly averages of: (**a**) air temperature; (**b**) relative humidity; (**c**) wind speed; (**e**) soil temperature; (**f**) soil volume water content (VWC); and (**d**) cumulative precipitation. GC is *Lyceum barbarum* cropland in Golmud, SL is shrubland of *Tamarix chinensis* and wild *Lycium barbarum*, NC is *Lyceum barbarum* cropland in Nuomuhong, and AM is alpine meadow.

3.2. Variation Characteristics of Evapotranspiration on Different Underlying Surfaces

3.2.1. Variation Characteristics of Evapotranspiration at Different Time Scales

Figure 3 shows the monthly changes of the actual ET at the four observation stations in the Qaidam Basin in 2020. Between April and October, the ET of the four observation stations as a whole showed a normal distribution and was mainly concentrated during the growing season, but there were also certain differences. The relationship between the total ET of the four underlying surfaces was NC > AM > GC > SL. The GC and AM had the highest ET in July at 62.50 mm and 88.92 mm, respectively, while the SL and NC had the highest ET in August at 40.47 mm and 100.02 mm, respectively. In addition, the ET of the AM was greater than that of NC before July and less than that of NC, and both observation stations had greater ET than GC and SL, while GC had greater ET than SL.

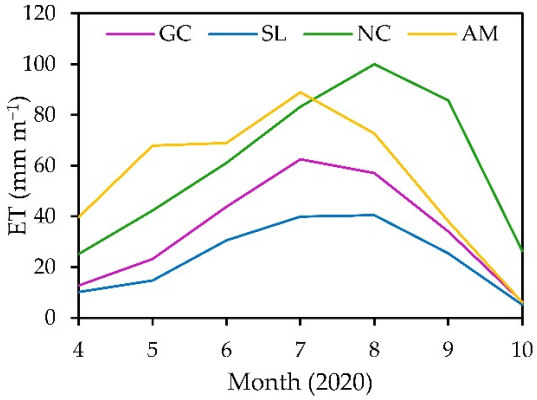

Figure 3. Trends of monthly evapotranspiration at the four observation stations in the Qaidam Basin in 2020.

Figure 4 shows the daily changes in the actual ET at the four observation stations in the Qaidam Basin in 2020. The actual daily ET at the four observation stations showed a trend of initially increasing and then decreasing. Moreover, the ET volatilities of NC and AM were greater than those of GC and SL. Among them, the average daily ET of GC was 1.12 mm and the maximum ET was 2.94 mm, which appeared on 27 June, and the minimum value was 0.03 mm, which appeared on 3 April. The ET began to increase slowly in April, showed a rapid increasing trend in May and June, reached a maximum value in July, and began to decrease in September. The average daily ET of SL was 0.78 mm, the daily maximum was 2.43 mm, which appeared on 21 June, and the daily minimum was 0.05 mm, which appeared on 29 October. The ET slowly increased from April to May, showed a rapid increasing trend from June onwards, and gradually decreased starting in September. The average daily ET of NC was 1.98 mm, the daily maximum was 4.46 mm, which appeared on 18 July, and the daily minimum was 0.26 mm, which appeared on 1 April. The ET showed a trend of increasing volatility starting in April and a declining trend starting in mid-September. The average daily ET of AM was 1.79 mm, the daily maximum was 4.45 mm, which appeared on 24 June, and the daily minimum was 0.03 mm, which appeared on 23 October. The ET showed a trend of increasing volatility starting in April and gradually declined since September.

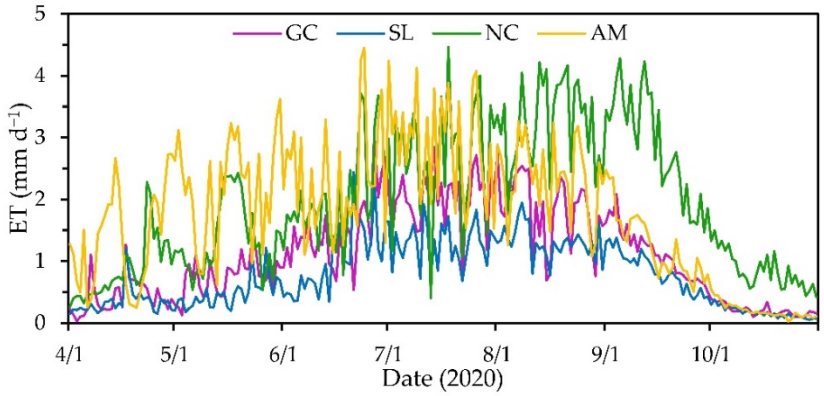

Figure 4. Trends of daily evapotranspiration at the four observation stations in the Qaidam Basin in 2020.

Figure 5 shows the half-hourly changes of the actual ET at the four observation stations in the Qaidam Basin in 2020. The daily change of ET over half an hour at the four observation stations showed a general trend of first rising and then declining. The ET was mainly concentrated from 9:00 to 20:00. Among them, the GC reached its peak of 0.060 mm around 14:00, SL peaked at 0.045 mm around 15:00, NC reached its peak of 0.110 mm around 14:30, and AM peaked at 0.106 mm around 14:30.

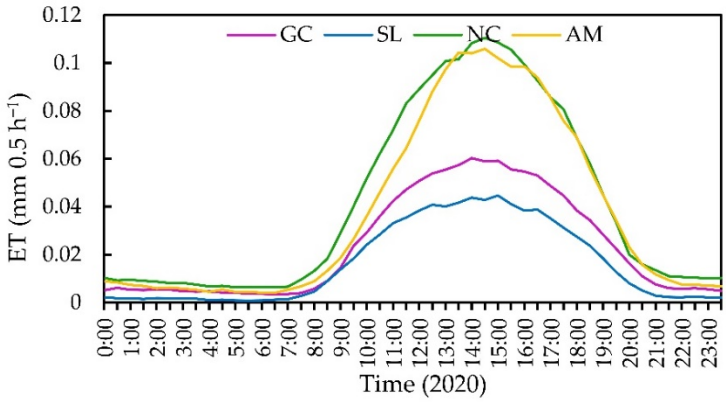

Figure 5. Trends of half-hourly evapotranspiration at the four observation stations in the Qaidam Basin in 2020.

This study found that the meteorological factors of GC and NC, which represent artificial surfaces, were not much different (as shown in Figure 2); however, the total ET of NC was 184.24 mm higher than that of GC. The field investigation indicated that the fundamental reason for this discrepancy is the different irrigation methods, with GC using drip irrigation and NC using flood irrigation. These differences in irrigation amount led to differences in ET. Wang et al. found that the maximum value of ET in cropland ecosystem was associated closely to the sufficient available water obtained by flood irrigation in the observation area of the HiWATER [14]. Flood irrigation may affect ET from two aspects. Flood irrigation may affect ET from two aspects. On the one hand, it can change the physiological process of vegetation by regulating water status, and on the other hand, it can increase the ET of the whole ecosystem by increasing surface evaporation [42]. As a natural underlying surface, the total ET of the AM was 215.89 mm higher than that of the SL, which was similar to the results of previous studies [35]. In addition to the differences in vegetation type, the meteorological factors between AM and SL were very different (as shown in Figure 2), which eventually led to differences in ET.

3.2.2. Correlation between Daily Evapotranspiration and Meteorological Factors

Table 2 shows the correlation between the actual daily ET and different meteorological factors (air temperature, relative humidity, wind speed, soil temperature, and soil volume water content) at four observation stations in the Qaidam Basin in 2020. The actual daily ET of the four observation stations was significantly correlated with air temperature ($p < 0.01$), and the correlation coefficient was very high. The actual daily ET of GC, SL, and AM was significantly correlated with relative humidity ($p < 0.01$), whereas the correlation coefficient of NC was relatively low. The correlation between actual ET and wind speed at all observation stations was not apparent; only the correlation coefficient of the GC observation station passed the $p < 0.01$ significance test, and they all showed a negative correlation. The actual daily ET of GC, SL, and AM was significantly correlated with the soil temperature ($p < 0.01$), and the correlation coefficient was very high. The actual ET of GC and AM was significantly correlated with soil volume water content ($p < 0.01$), and the correlation coefficient of AM was higher than that of SL.

Different ET mechanisms were affected by different meteorological factors. The variation in ET on different underlying surfaces in the Qaidam Basin is jointly affected by various meteorological factors. Air temperature and soil temperature were strongly correlated with ET and represented the main driving factors affecting the ET on different underlying surfaces. The movement of water molecules was more intense with an increase in temperature, and the ET intensity increased accordingly [43]. The relative humidity of the air is an important factor affecting ET. Many studies have shown that relative humidity was negatively correlated with ET [44,45]. Water vapor in the air is conducive to the occurrence of ET; however, when the relative humidity exceeds a certain range, it is not conducive to

the occurrence of ET. In this study, the relative humidity of the four underlying surfaces in Qaidam Basin was small, so the relative humidity was positively correlated with ET. The correlation between the ET of each underlying surface and wind speed was not strong, indicating that wind, as a driving factor, has little influence on ET [46]. In arid and semi-arid areas, soil volume water content (VWC) plays a significant role in controlling ET [47], and the ET of the AM and SL was strongly correlated with the soil volume water content (VWC).

Table 2. Correlation between actual evapotranspiration and different meteorological factors at the four observation stations in The Qaidam Basin.

Surface Type	Air Temperature	Relative Humidity	Wind Speed	Soil Temperature	VWC
GC	0.851 **	0.207 **	−0.189 **	0.841 **	0.242 **
SL	0.754 **	0.457 **	−0.040	0.782 **	-
NC	0.761 **	0.162 *	−0.133	-	-
AM	0.599 **	0.199 **	−0.042	0.592 **	0.667 **

Note: ** and * indicate significant correlation at $p < 0.01$ and $p < 0.05$ levels (bilateral), respectively.

3.3. Variation Characteristics of Water Consumption on Different Underlying Surfaces

The time series of daily ET and precipitation for the four underlying surfaces for the 2020 growing season are shown in Figure 6. Within a certain range, an increase in precipitation tended to increase the ET in GC, SL, and NC. However, when the precipitation increased to a certain threshold, the ET tended to decrease in AM, especially in June.

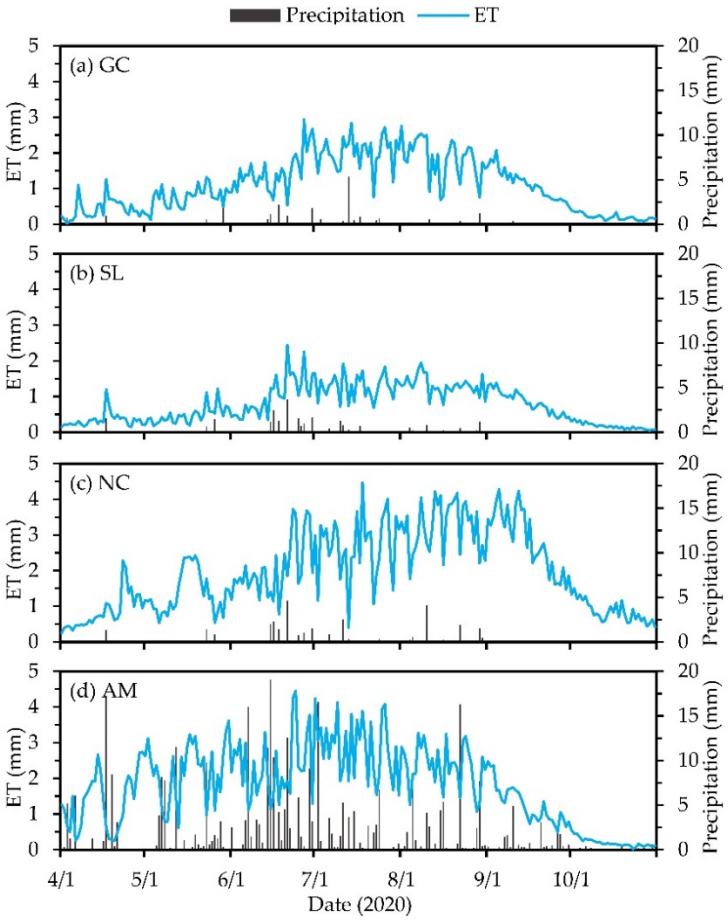

Figure 6. Temporal variation of evapotranspiration and precipitation at the four observation stations in the Qaidam Basin in 2020.

From 1 April to 31 October, the IETP (the difference between ET and precipitation) of GC, SL, NC, and AM was positive for 207, 206, 206, and 159 days (Figure 7) and had values of 96.73%, 96.26%, 96.26%, and 74.30%, respectively. This finding indicated that water consumption is the main factor of the four underlying surfaces most of the time. Water absorption occurred over a greater number of days on the underlying surface of AM compared with the other three areas, and the water consumption of the different underlying surface in the growing season was ordered as NC > GC > SL > AM, which had values of 394.03 mm, 217.69 mm, 142.68 mm, and 35.78 mm, respectively. This trend reflects the greater precipitation frequency and amount in AM (Figure 6). Therefore, when precipitation is lacking or decreased, the underlying surface is dominated by water consumption, and when precipitation is adequate or increased, the underlying surface is dominated by water absorption.

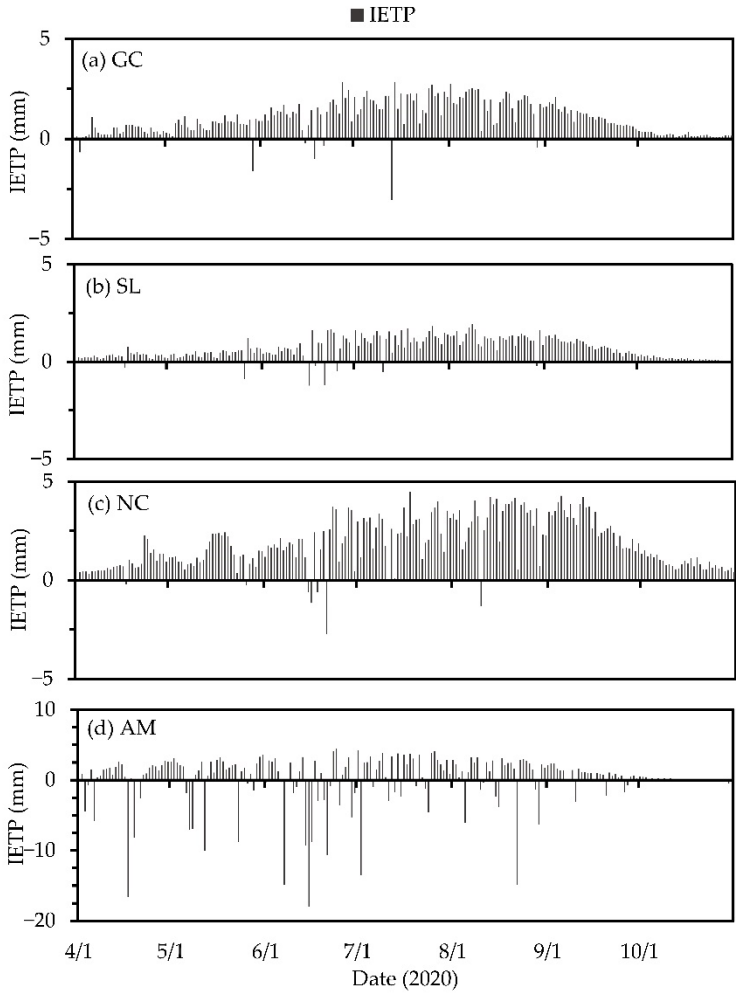

Figure 7. Change characteristics of IETP (the difference between ET and precipitation) at four observation stations in the Qaidam Basin in 2020.

This study used AM as an example to analyze the changing trends of IETP and meteorological factors, and the results are shown in Figure 8. The effects of meteorological factors on the IETP showed that the precipitation process led to a decrease in air temperature and soil temperature and an increase in relative humidity on the same day, thus inhibiting ET activity on the underlying surface. At this time, the underlying surface was dominated by water absorption, whereas when opposite conditions prevailed, the underlying surface was dominated by water consumption. The soil volumetric water content initially increased and then decreased with precipitation, which affected the ET.

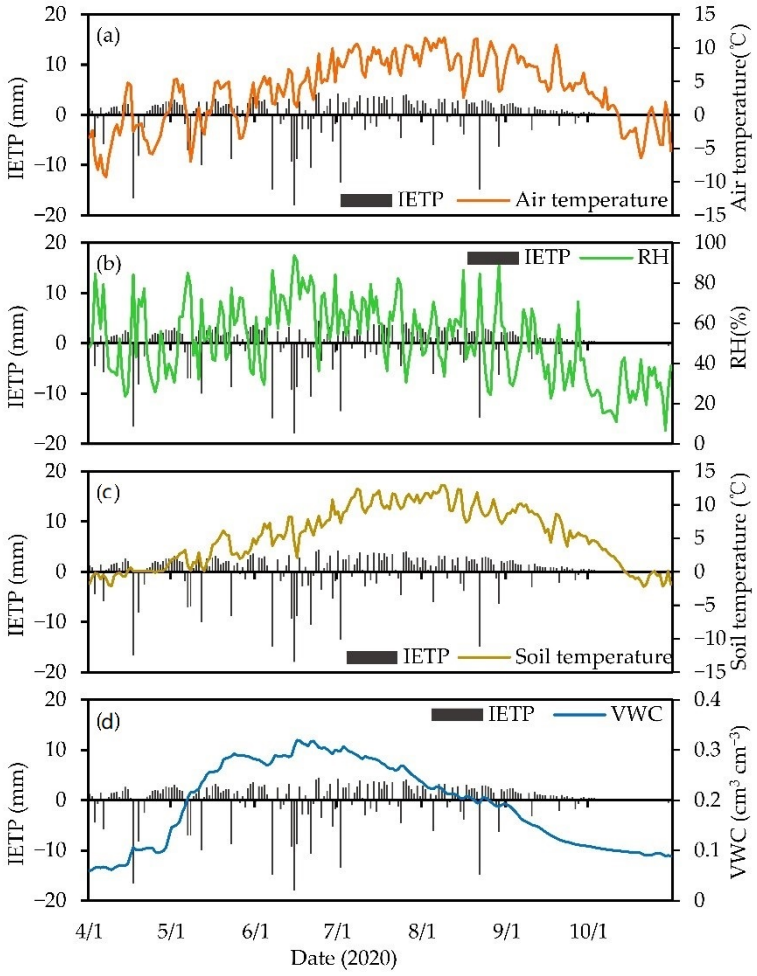

Figure 8. Trends of IETP and meteorological factors, including: (**a**) air temperature; (**b**) relative humility (RH); (**c**) soil temperature; and (**d**) soil volume water content (VWC), in AM.

4. Conclusions

In this study, EC observation data collected from systems installed on four underlying surfaces in the Qaidam Basin were selected to analyze the ET characteristics of each underlying surface at different time scales, explore the influence of different meteorological factors on the ET of each underlying surface, and analyze the water consumption characteristics of different underlying surfaces. The main conclusions are as follows.

The ET of the different underlying surfaces in the Qaidam Basin was mainly concentrated during the growing season in 2020. The overall monthly ET of the different underlying surfaces was normally distributed, with GC and AM having the highest ET in July and SL and NC having the highest ET in August. The average daily ET values for GC, SL, NC, and AM were 0.78 mm, 0.78 mm, 1.98 mm, and 1.79 mm, respectively. The half-hour ET reached its highest value between 14:00 and 15:00. The ET of different underlying surfaces in the Qaidam Basin was strongly correlated with air temperature and soil temperature, followed by relative humidity, while it was weakly correlated with wind speed. In addition, the daily ET of GC, SL, and AM was highly correlated with the soil temperature, and the daily ET of shrubland and alpine meadow was also highly correlated with the soil volumetric water content.

An analysis of the variation characteristics of water consumption on different underlying surfaces showed that the four underlying surfaces were dominated by water consumption, accounting for 96.73%, 96.26%, 96.26%, 74.30% in GC, SL, NC, and AM, respectively. Precipitation is the main input term for water balance. From the perspective of the variation law of precipitation and ET, when precipitation was lacking, the ET

was strong under increases in temperature and the underlying surface was dominated by water consumption. Within a certain range, an increase in precipitation was conducive to the occurrence of ET. However, when it exceeded a certain threshold, the temperature decreased and the relative humidity increased, thereby inhibiting ET. In addition, the soil accumulated water and the underlying surface was mainly dominated by water absorption.

The study on the actual ET of different underlying surfaces in Qaidam Basin is of great significance for the in-depth understanding of the water cycle in the alpine arid inland basin. Moreover, this work will provide a certain reference for the model simulation of ET in this area. The quantitative study of actual ET in Qaidam Basin can provide some basis for the rational allocation of local water resources and environmental protection. Due to the limited observational data, the four underlying surfaces in this study can't represent the ET characteristics of the entire Qaidam Basin. Therefore, it is necessary to further combine the measured data with remote sensing to obtain the characteristics of ET at the regional scale in the Qaidam Basin. In addition, only linear correlation was used in the analysis of the correlation between ET and meteorological factors in this study, and nonlinear correlation should be considered in future studies.

Author Contributions: Conceptualization, Y.W. and X.J.; methodology, Y.W.; software, Y.W.; validation, Q.M., C.H., Y.W. and X.J.; formal analysis, Y.W.; investigation, Y.W. and X.J.; writing original draft preparation, Y.W.; writing—review and editing, Y.W., C.H. and Q.M.; supervision, C.H. and Q.M. and X.J.; project administration, X.J.; funding acquisition, X.J. All authors have read and agreed to the published version of the manuscript.

Funding: This research was funded by Key Deployment Project of Chinese Academy of Sciences (ZDRW-ZS-2019-3, ZDRW-ZS-2020-3); National Key R&D Program (2018YFC0406600).

Data Availability Statement: The data presented in this study are available on request from the first author.

Acknowledgments: We thank the researchers and students of the National Key R&D Project, and the teachers and students of the Desert and Desertification Research Laboratory for their help. We thank the editors and reviewers for their insightful and valuable comments.

Conflicts of Interest: The authors declare no conflict of interest.

References

1. Xiao, J.F.; Sun, G.; Chen, J.Q.; Chen, H.; Chen, S.P.; Dong, G.; Gao, S.H.; Guo, H.Q.; Guo, J.X.; Han, S.J. Carbon fluxes, evapotranspiration, and water use efficiency of terrestrial ecosystems in China. *Agr. Forest Meteorol.* **2013**, *182*, 76–90. [CrossRef]
2. Avissar, R.; Schmidt, T. An evaluation of the scale at which ground-surface heat flux patchiness affects the convective boundary layer using large-eddy simulations. *J Atmos. Sci.* **1998**, *55*, 2666–2689. [CrossRef]
3. Zhang, B.Z.; Xu, D.; Liu, Y.; Li, F.S.; Cai, J.B.; Du, L.J. Multi-scale evapotranspiration of summer maize and the controlling meteorological factors in north China. *Agr. Forest Meteorol.* **2016**, *216*, 1–12. [CrossRef]
4. Xin, Z.B.; Xu, J.X.; Zheng, W. Spatiotemporal variations of vegetation cover on the Chinese Loess Plateau (1981-2006): Impacts of climate changes and human activities. *Sci. China Ser. D* **2008**, *51*, 67–78. [CrossRef]
5. Delgado-Baquerizo, M.; Maestre, F.T.; Gallardol, A.; Bowker, M.A.; Wallenstein, M.D.; Quero, J.L.; Ochoa, V.; Gozalo, B.; Garcia-Gomez, M.; Soliveres, S. Decoupling of soil nutrient cycles as a function of aridity in global drylands. *Nature* **2013**, *502*, 672–676. [CrossRef]
6. Rivas, R.; Caselles, V. A simplified equation to estimate spatial reference evaporation from remote sensing-based surface temperature and local meteorological data. *Remote Sens. Environ.* **2004**, *93*, 68–76. [CrossRef]
7. Trenberth, K.E.; Fasullo, J.T.; Kiehl, J. Earth's Global Energy Budget. *Bull. Am. Meteorol. Soc.* **2009**, *90*, 311–323. [CrossRef]
8. Wilcox, B.P.; Breshears, D.D.; Seyfried, M.S.; Trimble, S. Rangelands, water balance on. In *Encyclopedia of water Science*, 2nd ed.; Stewart, B.A., Terry, H., Eds.; CRC Press: Boca Raton, FL, USA, 2003; Volume 4, pp. 791–794. Available online: https://www.taylorfrancis.com/chapters/edit/10.1081/E-EWS2-240/rangelands-water-balance-bradford-wilcox-david-breshears-mark-seyfried (accessed on 27 September 2022).
9. Jin, X.M.; Guo, R.H.; Xia, W. Distribution of Actual Evapotranspiration over Qaidam Basin, an Arid Area in China. *Remote Sens.* **2013**, *5*, 6976–6996. [CrossRef]
10. Lemeur, R.; Zhang, L. Evaluation of three evapotranspiration models in terms of their applicability for an arid region. *J. Hydrol.* **1990**, *114*, 395–411. [CrossRef]

11. Yuan, G.F.; Luo, Y.; Shao, M.A.; Zhang, P.; Zhu, X.C. Evapotranspiration and its main controlling mechanism over the desert riparian forests in the lower Tarim River Basin. *Science China Earth Sciences.* **2015**, *58*, 1032–1042. Available online: https://link.springer.com/article/10.1007/s11430-014-5045-7#citeas (accessed on 27 September 2022). [CrossRef]
12. Hanson, R.L. Evapotranspiration and droughts. In *National Water Summary 1988–89: Hydrologic Events and Floods and Droughts*; Paulson, R.W., Chase, E.B., Roberts, R.S., Moody, D.W., Eds.; Geological Survey Water-Supply Paper 2375; U.S. Geological Survey: Reston, VA, USA, 1991; pp. 99–104.
13. Li, J.; Jiang, S.; Wang, B.; Jiang, W.W.; Tang, Y.H.; Du, M.Y.; Gu, S. Evapotranspiration and Its Energy Exchange in Alpine Meadow Ecosystem on the Qinghai-Tibetan Plateau. *J. Integr. Agr.* **2013**, *12*, 1396–1401. [CrossRef]
14. Wang, W.Z.; Xu, F.A.; Wang, J.M. Energy Exchange and Evapotranspiration over the Ejina Oasis Riparian Forest Ecosystem with Different Land-Cover Types. *Water* **2021**, *13*, 3424. [CrossRef]
15. Wang, Z.L.; Xie, P.W.; Lai, C.G.; Chen, X.H.; Wu, X.S.; Zeng, Z.Y.; Li, J. Spatiotemporal variability of reference evapotranspiration and contributing climatic factors in China during 1961–2013. *J. Hydrol.* **2017**, *544*, 97–108. [CrossRef]
16. Kim, H.W.; Hwang, K.; Mu, Q.; Lee, S.O.; Choi, M. Validation of MODIS 16 Global Terrestrial Evapotranspiration Products in Various Climates and Land Cover Types in Asia. *Ksce J. Civ. Eng.* **2012**, *16*, 229–238. [CrossRef]
17. Zhang, K.X.; Pan, S.M.; Zhang, W.; Xu, Y.H.; Cao, L.G.; Hao, Y.P.; Wang, Y. Influence of climate change on reference evapotranspiration and aridity index and their temporal-spatial variations in the Yellow River Basin, China, from 1961 to 2012. *Quatern. Int.* **2015**, *380*, 75–82. [CrossRef]
18. Douglas, E.M.; Jacobs, J.M.; Sumner, D.M.; Ray, R.L. A comparison of models for estimating potential evapotranspiration for Florida land cover types. *J. Hydrol.* **2009**, *373*, 366–376. [CrossRef]
19. Srivastava, A.; Sahoo, B.; Raghuwanshi, N. Evaluation of Variable Infiltration Capacity model and MODIS-Terra satellite-derived grid-scale evapotranspiration. *J. Irrig. Drain. Eng.* **2017**, *143*, 1-1. [CrossRef]
20. Chen, J.M.; Liu, J. Evolution of evapotranspiration models using thermal and shortwave remote sensing data. *Remote Sens. Environ.* **2020**, *237*, 111594. [CrossRef]
21. Sobrino, J.; Gómez, M.; Jiménez-Muñoz, J.; Olioso, A. Application of a simple algorithm to estimate daily evapotranspiration from NOAA–AVHRR images for the Iberian Peninsula. *Remote Sens. Environ.* **2007**, *110*, 139–148. [CrossRef]
22. Kalma, J.D.; McVicar, T.R.; McCabe, M.F. Estimating Land Surface Evaporation: A Review of Methods Using Remotely Sensed Surface Temperature Data. *Surv. Geophys.* **2008**, *29*, 421–469. [CrossRef]
23. Li, Z.L.; Tang, R.L.; Wan, Z.M.; Bi, Y.Y.; Zhou, C.H.; Tang, B.H.; Yan, G.J.; Zhang, X.Y. A Review of Current Methodologies for Regional Evapotranspiration Estimation from Remotely Sensed Data. *Sensors* **2009**, *9*, 3801–3853. [CrossRef] [PubMed]
24. Allen, R.G.; Pereira, L.S.; Howell, T.A.; Jensen, M.E. Evapotranspiration information reporting: I. Factors governing measurement accuracy. *Agr. Water Manag.* **2011**, *98*, 899–920. [CrossRef]
25. Yang, J.; Li, B.; Shiping, L. A large weighing lysimeter for evapotranspiration and soil-water–groundwater exchange studies. *Hydrol. Process.* **2000**, *14*, 1887–1897. [CrossRef]
26. Zabransky, P.; Pivec, J.; Brant, V.; Kroulik, M.; Skerikova, M. The Values of Crop Coefficients and Bowen Ratio of Field Crops in Areas with Insufficient Precipitation in Central Europe. *Irrig. Drain.* **2015**, *64*, 253–262. [CrossRef]
27. Williams, D.G.; Cable, W.; Hultine, K.; Hoedjes, J.C.B.; Yepez, E.A.; Simonneaux, V.; Er-Raki, S.; Boulet, G.; de Bruin, H.A.R.; Chehbouni, A. Evapotranspiration components determined by stable isotope, sap flow and eddy covariance techniques. *Agr. Forest Meteorol.* **2004**, *125*, 241–258. [CrossRef]
28. Baldocchi, D.; Falge, E.; Gu, L.H.; Olson, R.; Hollinger, D.; Running, S.; Anthoni, P.; Bernhofer, C.; Davis, K.; Evans, R. FLUXNET: A new tool to study the temporal and spatial variability of ecosystem-scale carbon dioxide, water vapor, and energy flux densities. *Bull. Am. Meteorol. Soc.* **2001**, *82*, 2415–2434. [CrossRef]
29. Baldocchi, D.D.; Hicks, B.B.; Meyers, T.P. Measuring Biosphere-Atmosphere Exchanges of Biologically Related Gases with Micrometeorological Methods. *Ecology* **1988**, *69*, 1331–1340. [CrossRef]
30. Ding, R.S.; Kang, S.Z.; Li, F.S.; Zhang, Y.Q.; Tong, L. Evapotranspiration measurement and estimation using modified Priestley-Taylor model in an irrigated maize field with mulching. *Agr. Forest Meteorol.* **2013**, *168*, 140–148. [CrossRef]
31. Law, B.E.; Falge, E.; Gu, L.; Baldocchi, D.D.; Bakwin, P.; Berbigier, P.; Davis, K.; Dolman, A.J.; Falk, M.; Fuentes, J.D. Environmental controls over carbon dioxide and water vapor exchange of terrestrial vegetation. *Agr. Forest Meteorol.* **2002**, *113*, 97–120. [CrossRef]
32. Lei, H.M.; Yang, D.W. Interannual and seasonal variability in evapotranspiration and energy partitioning over an irrigated cropland in the North China Plain. *Agr. Forest Meteorol.* **2010**, *150*, 581–589. [CrossRef]
33. Baldocchi, D.D. Assessing the eddy covariance technique for evaluating carbon dioxide exchange rates of ecosystems: Past, present and future. *Global Change Biol.* **2003**, *9*, 479–492. [CrossRef]
34. Xu, F.N.; Wang, W.Z.; Wang, J.M.; Xu, Z.W.; Qi, Y.; Wu, Y.R. Area-averaged evapotranspiration over a heterogeneous land surface: Aggregation of multi-point EC flux measurements with a high-resolution land-cover map and footprint analysis. *Hydrol. Earth Syst. Sci.* **2017**, *21*, 4037–4051. [CrossRef]
35. Guo, R.; Jin, X.; Wang, X.; Hu, G. Actual evapotranspiration estimation in Qaidam Basin based on Moderate Resolution Imaging. *Earth Sci. Front.* **2014**, *21*, 107–114.
36. Zhang, J.; Ren, Z. Analysis on Surface Spatiotemporal Variation Tendency of Potential Evapotranspiration in Qaidam Basin. *Resourc Sci.* **2014**, *10*, 2103–2112.

37. Zhu, W.; Lv, A.; Jia, S. Study on Spatial Distribution of Vegetation Coverage and Its Affecting Factors in the Qaidam Basin Based on NDVI. *Arid. Zone Res.* **2010**, *27*, 8.
38. Wang, J.M.; Zhuang, J.X.; Wang, W.Z.; Liu, S.M.; Xu, Z.W. Assessment of Uncertainties in Eddy Covariance Flux Measurement Based on Intensive Flux Matrix of HiWATER-MUSOEXE. *IEEE Geosci. Remote Sens. Lett.* **2015**, *12*, 259–263. [CrossRef]
39. Blanken, P.D.; Black, T.A.; Neumann, H.H.; Den Hartog, G.; Yang, P.C.; Nesic, Z.; Staebler, R.; Chen, W.; Novak, M.D. Turbulent flux measurements above and below the overstory of a boreal aspen forest. *Bound.-Layer Meteorol.* **1998**, *89*, 109–140. [CrossRef]
40. Falge, E.; Baldocchi, D.; Olson, R.; Anthoni, P.; Aubinet, M.; Bernhofer, C.; Burba, G.; Ceulemans, R.; Clement, R.; Dolman, H. Gap filling strategies for defensible annual sums of net ecosystem exchange. *Agr. Forest Meteorol.* **2001**, *107*, 43–69. [CrossRef]
41. Wang, J.; Zhang, R.; Li, H.; Lu, H.; Cao, X.; Liu, R. Relationship between water consumption and meteorology-vegetation parameters in the desert grassland on different time scales. *Agric. Res.Arid. Areas* **2020**, *38*, 152–158, 167.
42. Ma, X.; Feng, Q. Energy partitioning and evapotranspiration of Populus euphratica forests in desert riparian area. *Acta Ecol. Sin.* **2020**, *40*, 8683–8693.
43. Singer, K.D.; Kuzyk, M.G.; Sohn, J.E. Second-order nonlinear-optical processes in orientationally ordered materials: Relationship between molecular and macroscopic properties. *JOSA B* **1987**, *4*, 968–976. [CrossRef]
44. Chen, L.; Zhang, X.; Wang, Y.; Gao, M.; Tang, J. Temporal characteristics and influencing factors of evapotranspiration and water use efficiency on sloping farmlands with purple soil. *Chin. J. Eco-Agric.* **2021**, *29*, 991–1007.
45. Xiuying, W.; Bingrong, Z.; Qi, C.; Fu, L.; Chen, Q. Study onWater Consumption Law of Typical Alpine Meadow and Alpine SwampWetland Vegetation in Qinghai-Xizang Plateau. *Plateau Meteorol.* **2022**, *41*, 338–348.
46. Huang, H.; Cao, M.; Song, J.; Han, Y.; Chen, S. Temporal and Spatial Changes of Potential Evapotranspiration and Its Influencing Factors in China from 1957 to 2012. *J. Nat. Resour.* **2015**, *30*, 315–326.
47. Yang, F.L.; Zhou, G.S. Characteristics and modeling of evapotranspiration over a temperate desert steppe in Inner Mongolia, China. *J. Hydrol.* **2011**, *396*, 139–147. [CrossRef]